Construction and Building Materials 444 (2024) 137714

Contents lists available at ScienceDirect

Construction and Building Materials

journal homepage: www.elsevier.com/locate/conbuildmat

Correlation through directional statistics of the consequences of magnetic alignment of steel fibers immersed in metaphor fluids of cementitious matrices☆

Víctor Pérez Villar, Nelson Flores Medina *, Laura Trigo Ramirez

Departamento de Construcción Arquitectónica, Campus Universitario de Tafira s/n, Las Palmas de Gran Canaria, 35017, Gran Canaria, Spain

ARTICLE INFO

MSC:
76A10
78A25
82D40
74E30
74A40
62H11

Keywords:
Steel fiber alignment
Magnetic alignment
Circular statistics
Rheology cementitious materials
Fiber alignment management

ABSTRACT

Conceptually, the alignment of fibers in cementitious matrices leads to an appropriate choice of orientation indices, orientation coefficient, orientation tensors, etc. methods that do not have the advantages offered by descriptive or inferential statistics. The work presented here uses directional statistics as an efficient measure of the alignment of a set of fibers that initially have random orientations. The randomly oriented fibers are immersed in a *fluid metaphor* (hydrogel) transparent that reproduces some rheological characteristics of cementitious matrices. Magnetic alignment carried out by discharging an Resistor–Capacitor-Inductor-Circuit (RCL circuit) that causes pulses of homogeneous magnetic fields of intensity ranging approximately from 20 mT to 90 mT (peak) changing the final orientation distribution of the set of fibers. These changes in the orientation distribution give rise to their directional statistical analysis, revealing the relationships between the magnetic properties of the fibers and the rheological parameters of the matrix in which they are immersed. Among the studies presented here is the possibility of planning various fiber alignment strategies using a circular diagram as an abacus (Circles of Active/Dead Fibers) that allow us to go beyond the application of a simple pulse and/or a single alignment direction, seeking a process fiber alignment that is optimal and controlled.

1. Introduction

The alignment of steel fibers using magnetic fields is a relatively new branch within the area of cementitious composite materials. Being able to align fibers according to certain specific directions within a material increases its mechanical efficiency. Using a lower volume fraction of oriented reinforcing fibers, the same reinforcing effect is achieved if a larger volume fraction of the same disoriented (homogeneously distributed) fiber is used. The literature on this topic has been growing since the first decades after 2010, addressing different issues that come with the use of this technique. The first documented application for fiber alignment is due to Peterman [1] which uses magnetic fields to orient ferromagnetic particles in polymers. Under this same concept [2] uses electric fields to align cellulose fibers. The first application to the reinforcement of cementitious materials dates back to Miller and Björklund [3] using oscillating magnetic fields to 'facilitate' steel fiber orientation in forged architectural panels.

Magnetic fields in the early periods used electromagnets as a source, but it was not until Helmholtz Coils began to be used until there were homogeneous magnetic fields that showed greater efficiency in the alignment of ferromagnetic fiber. The first topic addressed is the use of homogeneous magnetic fields of different intensity that are usually in the range of 35 mT [4] up to 0.5 Teslas [5] using different kinds of coils (generally Helmholtz coils or geometric variants of such a coil). There are studies in which spatial arrangements of square magnets are used, seeking homogeneous magnetic fields with magnetic field intensities of 0.3 Teslas [6]. As a general rule, found in the scientific literature, exposures to homogeneous magnetic fields to directly align fiber does not vary over time, and are static.

Another important issue in fiber alignment research involving composite materials is the availability of direct measurement of fiber orientation. Most materials are opaque to visible light, and do not allow direct measurements of fiber angles. This is the reason why some fluid metaphors are used that reproduce some of the rheological properties, the most common is the static yield stress (τ_o). In the literature about fiber alignment some transparent 'metaphor fluids' are frequently used in this way [4] uses silicone oil to see the alignment effects of homogeneous magnetic fields ranging from 20 mT to 50 mT, Boulekbache et al. [7] uses hydrogeles like Carbopol, 'tuning' the value of the

☆ This document is the results of the research project funded by the National Science Foundation.
* Corresponding author.
E-mail addresses: victor.villar@ulpgc.es (V.P. Villar), nelson.flores@ulpgc.es (N.F. Medina), laura.trigo@ulpgc.es (L.T. Ramirez).

https://doi.org/10.1016/j.conbuildmat.2024.137714
Received 16 April 2024; Received in revised form 7 July 2024; Accepted 31 July 2024
Available online 10 August 2024

static tension through the pH of the solution or concentration. Some authors uses this hydrogel as a Bingham model in Spangenberg et al. [8] to reproduce cements mortars, and also Auernhammer et al. [9]. Being [10, sec. 4] a good summary showing a complete state of the art of recent uses of this hydrogel as a fluid metaphor for static yield stress.

In other research cases, direct measurement of fiber orientation is performed, e.g. using X-rays [4] allowing direct, three-dimensional measurement of the fiber orientation as a complement to the use of carbopol. Among the direct methods [11] performed a manual counting of the fibers to determine the quantity of fibers present in a cross section of the specimen, cutting the specimen and measuring the ellipsoidal section to deduce the orientation by geometric means.

In close relation to the difficulty of being able to directly measure fiber orientation angles, there is also a need to define an 'orientation index' capable of efficiently encoding the alignment of a spatial distribution of fibers. Some authors uses the fiber orientation number [12–15] as a single and simple parameter, indicating the percentage of fibers oriented in the cementitious matrix. This coefficient corresponds to the average projection of the unit vectors of the fibers on a desired direction.

The study of an orientation index, based on the modified rule of mixtures (aka Cox-Krenchel model) from Cox [16], Krenchel [17], extended to include the effect of fiber length and fiber orientation, uses the orientation efficiency factor (aka Krenchel factor) to predict some mechanical properties of composite materials based on fibers, eć et al. [18] give predictions for the tensile moduli of isotropic and oriented wood polymer composites (WPC), and Mu et al. [19] is a recent researcher who uses it in the study of the orientation of steel fiber on the strength of ultra-high-performance concrete (UHPC), being [20] a good review of this orientation factor that links mechanical properties with the 'statistical' orientation of the fiber.

2. Theoretical setup

The steel fiber is made of a ferromagnetic material that responds non-linearly to the presence of magnetic fields due to the existence of a hysteresis cycle. The magnetic response is characterized by a magnetic torque that aligns it, as long as the magnetic field is homogeneous. On the other hand, the fiber is immersed in a suspension or a fluid viscous matrix whose resistive response (also nonlinear) is characterized by the rheological properties of the fluid. To understand the complex nature of the aligning process of the steel fibers, it is necessary to understand and analyze in sufficient detail the relationship between the driving torque (magnetic) and the opposite torque (rheological) of the fluid that surrounds it.

2.1. Magnetic torque in steel fibers

The magnetic response of an elongated steel fiber to a homogeneous magnetic field in space $\vec{\mathbf{H}}$ is a magnetic torque $\vec{\tau}_M$ that causes the alignment of the magnetic axis of the steel fiber with the external magnetic field pointed out by a vector $\vec{\mathbf{H}}$ (A/m). The magnitude and direction of this magnetic torque is expressed by a vector cross product formula given by:

$$\vec{\tau}_M = \mu_\circ (\vec{\mathbf{m}}_f \times \vec{\mathbf{H}}) \qquad \Rightarrow \qquad |\vec{\tau}_M| = \mu_\circ |\vec{\mathbf{m}}_f| |\vec{\mathbf{H}}| \sin\theta \tag{1}$$

where $\mu_\circ$ is a universal constant called the magnetic permittivity of the vacuum, $\vec{\mathbf{H}}$ is the exciting homogeneous magnetic field, $\vec{\mathbf{m}}_f$ is the magnetic dipole moment of the fiber (A/m^2) [21, chap. 12] and θ is the angle between the magnetic axis of the steel fiber and the external magnetic field. The magnetic moment can be expressed as if it was the product of the length of the fiber ℓ and a 'theoretical' magnetic charge Q_m (A·m) located at the ends of the fiber, that is: $\vec{\mathbf{m}}_f = \ell Q_m$. The magnetic monopole can also be expressed as a product of the fiber section by the perpendicular induction field component $\vec{\mathbf{B}}_n$, therefore the expression for the magnetic moment of the fiber can be deduced as:

$$|\vec{\mathbf{m}}_f| = \ell\, S\, |\vec{\mathbf{B}}_n| \tag{2}$$

The relationship between the induced magnetic flux density ($\vec{\mathbf{B}}$) from the steel fiber magnetization and the magnetizing force ($\vec{\mathbf{H}}$) caused by external coil (in our case the Helmholtz coil) is a non-linear function characteristic of ferromagnetic materials called *hysteresis loop* where the magnetic induction B is proportional to $\mathcal{H}_B(H)$ [21, chap. 10]. Therefore, since the normal component of the magnetic field is given by $|\vec{\mathbf{H}}|\cos\theta$, the magnetic torque exerted to fiber has a final expression as a function of the exciting magnetic field $\vec{\mathbf{H}}$ like:

$$|\vec{\tau}_M| = \ell\, S\, |\vec{\mathbf{H}}|\ \mathcal{H}_B(|\vec{\mathbf{H}}|\cos\theta)\ \sin\theta \tag{3}$$

Where ℓ is the length of the steel fiber (m), and S the section (m^2), and θ the initial angle of the magnetic axis of the fiber with respect to the exciting homogeneous field $\vec{\mathbf{H}}$ that comes from the Helmholtz coil. It should be emphasized that the magnetic torque will depend directly on the volume of the fiber, in addition of being proportional to its θ orientation angle. The magnetic torque always is zero when the fiber is perpendicular to the exciting magnetic field $\vec{\mathbf{H}}$, that is, when the angle θ is equal to 90° and 0°, explained latter when commented Fig. 4.

Some authors have investigated the ferromagnetic properties of a set of steel fibers commonly used in industry, and provide parameters that characterize the hysteresis cycles that are common among them [22]. We consider relevant in this study the following three parameters of the hysteresis loop (see Fig. 1):

1. *Saturation induction* - B_m, which is the maximum magnetization that the fiber acquires. Due to the ferromagnetic materials used (steel) this value is around 1.6-1.7 Teslas. The fibers reach this saturation immediately, and most of the time the fiber dynamics are in this magnetic saturated state.
2. *Cohercitive field* - H_c, which is supposed to be the magnetic field that cancels the magnetic induction inside the fiber. This value in most fibers is around 200 A/m. This value, in steel fibers, is very narrow compared to other ferromagnetic materials.
3. *Intersection field* - H_i magnetic field magnitude at which the ascending/descending branches of the hysteresis loop intersect. For simplicity, this value has been taken equal to 800 A/m, consistent with the data presented in Künzel et al. [22].

The initial magnetization curve (o-a in Fig. 1 aka an hysteresis curve or virgin curve) is the magnetic state that runs through the fiber when it has not been previously magnetized, showing a linear relationship such that $B = \mu_o \mu_r H$ at $H \to 0$ A/m (very low magnetic fields). The value of μ_r the characteristic relative magnetic permeability of the material is around 550, which is a typical value for alloys of steel. The fiber goes through this initial o-a curve and reaches the saturation state immediately when the fiber is excited with magnetic field profiles associated with RCL magnetic pulses. Once the magnetic field ceases, the fiber becomes 'magnetized' with a *remanent induction* B_r (leter b in Fig. 1).

The complete hysteresis loop has been mathematically modeled in ferromagnetic materials [23,24], and can be used in software simulations of fiber alignments in order to determine the effect of certain ferromagnetic parameters on the alignment of steel fibers. The T(x) model developed by Takács [25] will be used here to cover most of the ferromagnetic behaviors of steel fibers. One branch of hysteresis loop is modeled as a linear combination of a hyperbolic tangent and a linear function as:

$$\mathrm{T(x)} = \mathrm{A}_o\, x + \mathrm{B}_o\ \tanh(\mathrm{C}_o\, x) \tag{4}$$

where A_o, B_o and C_o are parameters that define the magnetic response of the ferromagnetic material of the steel fiber and tanh is the hyperbolic tangent. We consider that $A_o \approx 0$, that is, B_o will be equal to

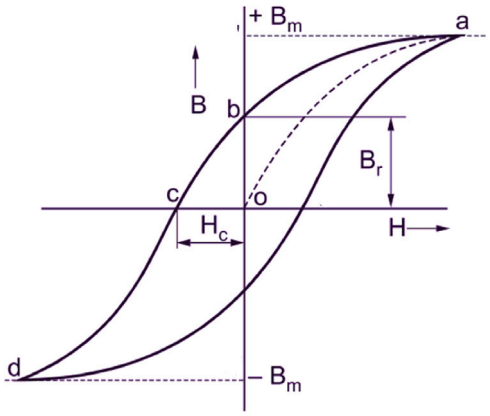

Fig. 1. Characteristic figure of a complete cycle of a steel fiber (ascending/descending loop), including the initial magnetization curve (o-a).

the saturation induction B_m. The parameter C_o in Eq. (4) is a scale parameter to be chosen appropriately to be fitted with the experimental data. In order to describe branches of the symmetric hysteresis loop, the hyperbolic part of T(x) is shifted in horizontal direction (to the right and left by H_c) and in vertical direction up and down by b_o according with the expression [25]:

$$b_o = \frac{1}{2}\ \left\{\tanh\left[C_o\left(H_i + H_c\right)\right] - \tanh\left[C_o\left(H_i - H_c\right)\right]\right\} \tag{5}$$

The ascending/descending branches depends of increasing/decreasing magnetic field

$$\mathcal{H}_B(H) \approx \begin{cases} B_m(\tanh\left[C_o\left(H - H_c\right)\right] + b_o) & \text{asc. branch} \\ B_m(\tanh\left[C_o\left(H + H_c\right)\right] - b_o) & \text{desc. branch} \end{cases} \tag{6}$$

With the four parameters that characterize the ferromagnetic properties of the steel fiber through the hysteresis cycle, that is: saturation induction B_m, cohercitive field H_c, the intersección of ascending/descending branches H_i and scale factor C_o. The hysteresis loop $\mathcal{H}_B(H)$ can be characterized according to Eq. (6). This characterized function allows determining the magnetic torque using (1).

Due to the magnitude of the magnetic pulse from the coil (greater than 30 mT peak), the fiber, according to the hysteresis loop, becomes saturated almost immediately. However, it is interesting to note that some fibers may have angle orientations θ so close to 90° whose cosine in the argument of the hysteresis function of the expression (3) of the magnetic torque is near to zero and cannot reach the magnetic saturation level (B_m in Fig. 1).

2.2. Rheological torque in steel fibers

The steel fiber, when immersed in a fluid matrix, is compelled to be aligned with the exciting homogeneus magnetic field $\vec{\mathbf{H}}$, but the rheological properties of the fluid matrix always are opposite to its movement. Thus, considering the rheological characteristics of the fluid matrix is relevant in any fiber alignment analysis. Cementitious matrices rheologically obey Bingham's law in most cases [26]. Structured fluids, such as concentrated suspensions and liquid crystals show rheological response as solid at low stress levels. In this rheological model, if τ is the shear stress and $\dot{\gamma}$ the shear rate, η is the plastic viscosity of the material, so in this way the Bingham's law is formulated as a constitutive equation: $\tau = \tau_o + \eta\dot{\gamma}$ if $\tau > \tau_o$. This type of fluid matrices that obey Binham's law have the relevant parameter which is the static yield stress τ_o which is understood in the present study as the energy per unit of volume (pressure) necessary to 'start 'the rotating movement of the fiber.

Because fiber rotation experiments will be carried out, it is necessary to directly measure the orientation angle of each fiber. This requirement needs a transparent material that simulates (at least) the static yield stress of a fluid mortar (or a fluid matrix of a composite). To carry out this fiber orientation measurement in this metaphor fluid (model fluid), it is necessary reproduce a specific value of τ_o, which in our case is Carbopol 940. However, this fluid obey to a Herschel–Bulkley law (H-B law) with constitutive equation $\tau = \tau_o + K\dot{\gamma}^n$, where τ_o is the static yield stress which will be the 'metaphor' used here. Parameters K and n in this H-B constitutive equation are other parameters that determine the rheological properties of carbopol.

This hydrogel is characterized and allows predicting the value of the static yield stress τ_o as a function of its pH and concentration. Because the production of the hydrogel sets the pH value to 7, τ_o can only be characterized by concentration. Jaworski et al. [10] proposes a $\tau_o(C)$ function expressed C in mass percentage concentration of carbopol, and τ_o in Pa, is given by two regimens:

$$\tau_o(C) = \begin{cases} \left(\dfrac{C}{0.0335} - 1\right)^3 & \text{for} \quad 0.045\% < C < 0.155\% \\ 45\sqrt[3]{\dfrac{C}{0.124}} & \text{for} \quad 0.155\% < C < 4.000\% \end{cases} \tag{7a}$$

Given this equation, and knowing the value of the magnetic driven torque, whose evolution is described in Fig. 4, the carbopol concentration value C of interest for the experiments to be carried out can be chosen.

2.3. Fiber dynamics

The study of fiber dynamics must consider two opposing effects. On the one hand, the effect caused by driving magnetic torque acting on fiber, which is determined by Eq. (3). The magnetic torque encodes a large proportion of the ferromagnetic properties of the steel fiber (hysteresis, magnetic moment, magnetic state, etc.). On the other hand, the rheological torque is opposed to the magnetic torque driver. The rheological torque encodes the properties of the fluid matrix surrounding the steel fiber.

Being able to know the nature of both opposite effects, it is decisive to explain the alignment of fibers through magnetic fields. Because magnetic torque has units of energy, so does rheological torque. Both expressions can be understood as the energy necessary/consumed to provide a change in rotational kinetic energy to the fiber that causes alignment to the fiber due their rotation. That is, the dynamics of the fiber can be described by the following equation:

$$\underbrace{\ell\, S\, |\vec{H}(t)|\, \mathcal{H}_B(|\vec{H}(t)|\, \cos\theta)\, \sin\theta}_{\text{Magnetic Torque}} = \underbrace{Y_R(S_{fo}, T_o^{(d)}, T_o^{(e)}, \dot{\theta})}_{\text{Rheological Torque}} + \underbrace{I\,\ddot{\theta}}_{\text{Inertia}} \tag{8}$$

In this equation, the rheological properties of the fluid act as a damper for the rotation movement, that is, they 'brake' the rotation caused by the magnetic torque until a final angular value is reached: θ_f (final orientation), which does not necessarily have to be zero (fully aligned fiber). On the other hand, the nonlinear condition is shown in several aspects within the equation: the fiber made with a ferromagnetic material (steel) has a hysteresis cycle as the main part of its magnetic response, and on the other hand the fluid shows a response of opposition with a characteristic threshold torque called static yield stress τ_o. There is no orientation rotation of the fiber until this threshold torque τ_o is exceeded, and this already predicts that some fibers, under this model, cannot be aligned.

2.4. Directional statistics

Directional statistics is that branch of statistical methodology specifically designed for use with observations that are directions [27], therefore is suitable for comparative measurements performed on fiber orientation data measurement. Let $\theta_1, \theta_2, \theta_3, \ldots \theta_n$ be a set of n fiber

orientations given in terms of angles. Consider the polar to rectangular transformation for each fiber observation:

$$(\sin\theta_i, \cos\theta_i) \quad i = 1, \ldots, n$$

the cartesian coordinates of the 'center of mass' $\vec{\mathbf{R}}$ are $(\hat{S}, \hat{C})$ expressed as:

$$\hat{S} = \frac{1}{n}\sum_{i=0}^{n}\sin\theta_i \qquad \hat{C} = \frac{1}{n}\sum_{i=0}^{n}\cos\theta_i \tag{9}$$

The fiber orientation number defined in Laranjeira et al. [12] it is precisely only the $\hat{C}$ value. Provided that $\hat{R} > 0$, where the mean resultant length R is given by:

$$\hat{R} = \left\|\vec{\mathbf{R}}\right\| = \sqrt{\hat{S}^2 + \hat{C}^2} \tag{10}$$

represent the length of the resultant vector R. The direction of this resultant vector $\vec{\mathbf{R}}$, which is proposed as the *circular mean orientation* of fibers, is denoted by $\bar{\theta}$, and is defined as:

$$\bar{\theta} = \arctan\left(\frac{\hat{S}}{\hat{C}}\right) \tag{11}$$

The first advantage of using $\bar{\theta}$ as a mean angle of fiber orientation, is that it has the property of being rotationally equivariant, i.e., if the data is shifted by a certain amount angle, the value $\bar{\theta}$ also changes by the same amount [28, p. 14,prop 1]. The invariant property of $\bar{\theta}$ and $\hat{R}$ against rotations allows, in our case, to plan sequences of fiber alignments in successive exposures to magnetic pulses, using different alignment directions.

The mean radius $\hat{R}$ is a useful measure for circular data, indicating how concentrated the fiber angles is towards this mean orientation $\hat{\theta}$. Directional statistics also is fully compatible with the composite orientation efficiency factor η_θ (aka the Krenchel factor) [16,29] used in the modified rule of mixtures

$$E_c = \eta_\theta \chi_f E_F + (1 - \chi_f) E_m \tag{12}$$

Where E_m, E_f and χ_f represent the moduli and volume fractions of the matrix and fiber respectively and E_c represents the modulus of composite. The rule of mixture model is suitable to estimate the tensile modulus of composites with aligned continuous fiber. This simple model assumes that there are equal strain experienced in both matrix and fiber. To compute the fiber orientation factor [29] proposes to be proportional to $\cos^4\theta$. To integrate this theory with directional statistics, if we divide the circumference into k bins, we have the :

$$\eta_{\theta_o} = \sum_k \chi_k \cos^4\left(\theta_k - \theta_o\right) \qquad \text{Where} \qquad \eta_\theta \in [0, 1] \tag{13}$$

Where χ_k is the proportion of total fiber angles content per bin and θ_k is the representative fiber angle per bin with respect to the loading direction θ_o. If the fibers are unidirectional (all set in one direction). with respect to the axis of loading. The reinforcement orientation distribution factor ranges between 0 (fibers aligned transverse to the stress direction) and 1 (fibers aligned parallel to the stress direction), the value of 3/8 (0.375) corresponds to randomly oriented fiber. FRC can be said to have η_θ=1 (100%) the maximum reinforcement level for cracks perpendicular to the direction of the fibers.

3. Experimental program

The materials used in the experimental procedure consist of a Helmholtz coil that generates uniform magnetic fields inside the coil, a current supply system connected to the coil and designed to be capable of generate intense current pulses in a short period of time, a transparent fluid whose rheological properties simulate 'some' (not all) of the rheological characteristics of the composite cementitious matrices (fluid metaphor), and finally three types of steel fibers commonly used in the industry.

The experiments are carried out in such a way that they are recorded by a digital camera to be subsequently digitally treated, measuring the angles of each steel fiber before/after being magnetically exposed.

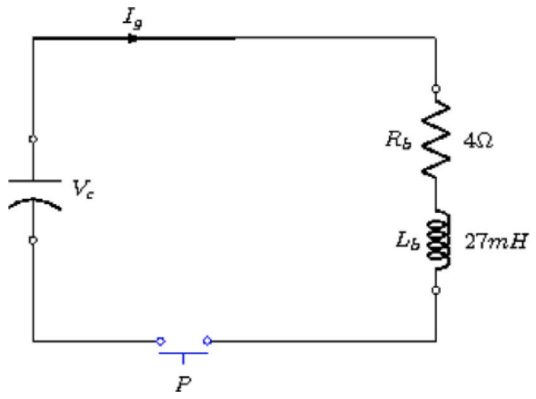

Fig. 2. RCL discharge circuit showing the coil inductance L_b and the internal impedance R_b.

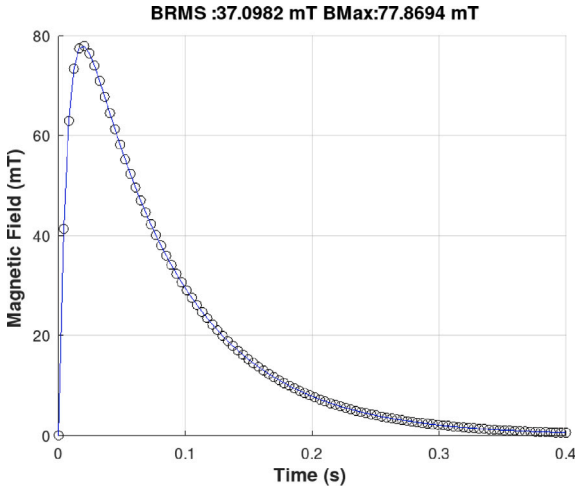

Fig. 3. RCL discharge of high peak intensity used in the experiments described here.

3.1. Description of the coil and circuits

The experimental procedure was designed in such a way that the device for generating homogeneous magnetic fields was a Helmholtz coil with a radius of 10.5 cm and 240 turns which has an inductance of 26.7 mH (see Fig. 2) and internal impedance of 4 Ω. The exposure of the samples to homogeneous magnetic fields is carried out in the interior space of the coil. The coil was electrically connected to a discharging circuit that used high-capacity electrolytic capacitors (as can see in Fig. 2). To control the peak intensity level, the voltage at terminals V_o of the capacitors was previously measured with a polimeter.

The higher the voltage at the capacitor terminals, the greater the peak discharge intensity on the coil. The terminals of the capacitors are connected to a charging circuit that has a direct current source that causes the capacitors to charge during a time interval. Once the desired charging voltage V_o value was reached, the capacitive discharge circuit was closed, producing a characteristic RCL discharge peak (as seen in Fig. 3).

The *discharge RCL circuit* was designed to generate an over-damped intensity pulse and the critical design parameter was the arrangement of the capacitors with a total capacity of 20.4 mF (see Fig. 2). The design of the RCL discharge circuit produces a maximum peak current at 0.016 s (approximately 20 hundredths of a second) descending in long a tail of intensity that lasts for 0.4 s. This peak occurs at the same instant in all the experiments described in the present work. Because a Helmholtz coil of known geometry is used, the generated magnetic

Table 1
Three types of RCL discharges used in the experiments.

Type	μ_oH (mT) Peak	RMS (mT)
Low	43.3	20.6
Medium	60.6	28.8
High	77.9	37.1

Table 2
Table with the three hooked-end fibers used (Courtesy of Bekaert).

(Bekaert Cod.)	ℓ (mm)	d (mm)	ℓ/d	m (g)
45/50/BL	51.38	0.90	57.09	0.29
65/60/BG	60.00	0.90	66.70	0.33
80/60/BG	60.00	0.75	80.00	0.22

field intensity is proportional to the discharge intensity, and therefore the magnetic pulse has the same shape as the discharge profile of the RCL circuit.

The magnetic exposure of all experiments described here have used three characteristic discharges whose peaks and RMS values are described in Table 1.

The coil is initially charged to a specific voltage V_o due to a grid-connected charging circuit. The 'trigger' occurs by short-circuiting the discharge circuit that literally 'dumps' all the electrical charge of the capacitors onto the coil. This mechanism has the advantage of producing a large amount of electrical intensity without causing great heating of the coil wires. The maximum voltage Vo that can be achieved will depend on the maximum rupture voltage of the capacitors.

3.2. Metaphor fluid preparation

Considering that the fiber can be included in a fluid cementitious matrix (cement paste or mortar) whose static yield stress ranges approximately between 15 - 125 Pa [26] and taking these value as a reference for Eq. (7a), a dilute carbopol solution of 0.2% is prepared assuming that the static stress could be approximately around 35 to 60 Pa [10] according with formula (7a) the carbopol used here has a theoretical value of static yield stress of 52.7 Pa.

The process of preparing the aqueous solution of carbopol begins with the dehydrated Carbopol powder which is first slowly added to distilled water through a fine metal mesh using a variable speed mixer. The solution is then neutralized by ethanolamine. A mixing period of 6 h follows this neutralization phase. Finally, the products are conserved at 25° C for a resting period of time: 24 h.

3.3. Fibers

Three types of commercial steel fibers from the Bekaert company, all of them within the Dramix ·D (hooked end fibers) category, are widely used in the construction industry. The three types defined in the experiments use the Bekaert code and the geometry associated with each fiber can be seen in Table 2.

The aspect ratio of all three fibers are $\ell/d > 50$ and all of the has a hooked-end geometry. Considering the ferromagnetic properties of the fibers, all of them are similar to each other, and were the subject of detailed discussion in previous section §2.1 of this work.

Considering the magnetic properties already mentioned for each type of fiber, it can be determined whether the magnetic torque response of the steel fibers is adequate by comparing it with some of the rheological properties of the fluid: specifically with its yield stress τ_o. To study this magnetic response, the (3) equation can be used for each fiber. As a sample example, Fig. 4 shows the case study for the magnetic torque of three types of fibers in medium intensity magnetic fields. Using the expression (1) to the fiber types defined (see Table 2), Fig. 4 is obtained. This figure represents the magnetic driving torque (N · mm) for the three types of steel fiber considered. The magnetic torque increases in the three types of fiber as it is oriented at an angle θ with respect to the magnetic axis, the magnetic torque of the coil always cancels out at 90 degrees. It should be noted that the magnetic torque reaches a maximum near 90 degrees and drops dramatically in an interval of just one or two degrees. It has been proven by simulation that ferromagnetic property of the cohercive field H_c in Fig. 1 produces this small interval of magnetic torque drop. It can be understood that this value should be as small as possible since it affects the maximum magnetic torque, for this reason small values of the cohercive field H_c maximize the alignment process. However, this cohercitive field seems to have a small fixed value of 200 A/m in the current fibers on the market [22].

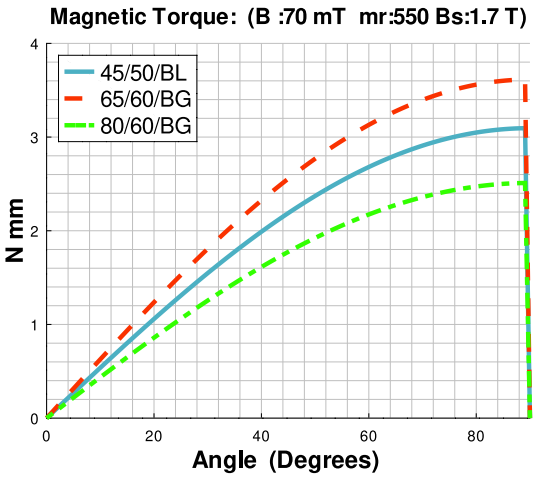

Fig. 4. Magnetic torque at different orientations from 0° to 90° considering the three types of fibers given in Table 2.

3.4. Experimental campaign & measurement

Six experimental campaigns have been carried out, two campaigns per type of steel fiber (see Table 2). For each type of fiber, the first campaign consists of exposure to three different magnetic field peaks according with Table 1 and the steel fiber was not initially magnetized (that is, the fiber did not have a remaining magnetic field), the second campaign was repeated with previously magnetized fibers following the same procedure. The set of experiments carried out for each campaign was photographed before and after being exposed to the magnetic field peaks; a digital camera located at the zenith (orthogonally from above) with respect to the sample was used to capture data. The technical characteristics digital camera are: Dual 12MP Wide and Ultra Wide with f/2.4 of apperture. An example of zenith photography for data capture is shown in Fig. 5, in which the angle measurements before/after the fibers are magnetically exposed are shown as an example. Angle measurements are carried out in batches of 5 randomly arranged fibers completely immersed in a container with carbopol, in different height planes in order to prevent initial contact between the fibers. Any contact between the fibers must be avoided because the mechanical and ferromagnetic characteristics of the set of fibers in contact alter the final orientation values. In the measurements carried out, those experiments that have been found that the fibers are into contact, or those that have been influenced by contact between the walls, are discarded. Some authors describe the contact network between rigid fibers inside the material [30]. Each fiber is arranged inside the container in a horizontal plane, thus guaranteeing that the movement of the fibers occurs completely in two dimensions. The time interval between the measurement of two successive batches exceeds one hour in all cases, considering that the fluid recovers its initial state during this rest

Fig. 5. Alignment process of measuring the angle θ before/after in Carbopol. Given three examples for each hooked-end steel fibers considered in Table 2. It can be seen that some dead fibers do not align while other active fibers can be oriented according to the axis of the coil.

interval. Fibers that have been radiated with magnetic fields, that is, they have magnetic remanence, are subsequently used in campaigns in which magnetized fibers are considered.

The campaign of non-magnetized fibers initially consists of approximately one hundred measurements, the second campaign of magnetized fibers is smaller and reaches only approximately thirty observations. The dataset obtained in the case of fiber with initial remanence (initially magnetized fiber) was made with the intention of qualitatively checking whether or not there were significant differences with the datasets from the campaign with initially non-magnetized fiber.

4. Experimental results

Considering that the datasets obtained by each fiber are arrays of angular data before/after, we have proceeded to treat them with descriptive circular statistics, calculating for each campaign the following statistics that are gathered in the tables in the Appendix:

1. N is the number of data used in the campaign.
2. The vector components $(\hat{S}, \hat{C})$ obtained according to the expression (9) in order to calculate the mean angular value $\bar{\theta}$ of the sample, as well as the measure of the angular dispersion R obtained form expression (10).

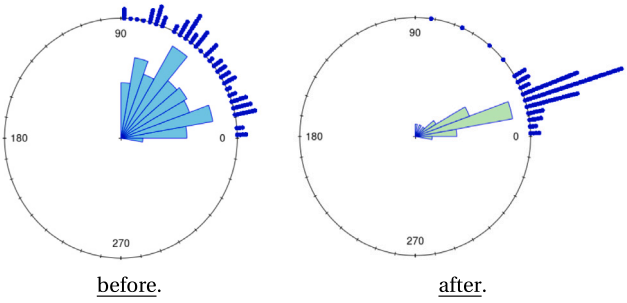

Fig. 6. Circular histogram taking bins of 5° to represent the alignment process before/after in Carbopol. Given example for 45-50 BL hooked-end steel fiber with low peak.

3. Measurements made on the cumulative distribution for the first quartile (25%), the median (50%), as well as for the third quartile (75%) and the fourth quartile (100%) are included.
4. the composite orientation efficiency factor η_θ (aka the Krenchel factor) calculated from (13) considering the axis of the coil as angular reference.

4.1. Angle before/after and response angle to the field H(t)

The empirical tasks carried out in the laboratory, each of the three types of fibers in Table 2 are exposed in sets of five fibers immersed in bucket of 300 cm^3 volume with carbopol (see Fig. 5). Fig. 7 represents three campaigns of 45/50/BL fiber exposed to magnetic fields with peaks: low, medium and high peaks according to Table 1. Each of the figures within the campaign represents on the abscissa axis the angle of the steel fiber before being exposed to the magnetic field (angle before) measured with respect to the magnetic axis of the coil by the shortest path. For this reason the range of angles of this axis covers only a domain from 0° (fiber fully aligned) to 90° (fiber perpendicular to the coil's magnetic axis).

The vertical ordinate axis indicates the final angles of each steel fiber after executing a coil pulse (angle after). Because the fibers always tend to align with the magnetic axis of the coil, the angles after the coil is 'triggered' are always less than, or equal, to the initial angles. A bisecting line is included dotted in each graph as a graphic reference. The points located on this bisecting line show, therefore, those steel fibers that have not undergone any change after exposure to the magnetic field from the coil.

Considering in depth the idea of the bisecting line as a reference (Fig. 7), those points that are on the bisector correspond to steel fibers that do not undergo a change in their orientation after a magnetic pulse (dead fibers), and in the same way those points (measurements) that are very far from the bisector have rotated in a greater change in orientation (active fibers). The greater its distance from the bisecting line, the greater the change that the fiber undergoes. Therefore, the distance with the bisecting line provides us with a quantification or measurement of the *fiber's response* to magnetic fields.

Taking into account that θ_o is the initial angle (before) and θ_f is the final angle of the steel fiber after the exposure of the magnetic field from the Helmholtz coil, the so-called response of the fiber will be proportional to the distance of the point $P(\theta_o, \theta_f)$ projected orthogonally to the bisector line b, that is:

$$d(P,b) = \frac{|\theta_o - \theta_f|}{\sqrt{2}} \quad \Rightarrow \quad \underbrace{(\theta_o, d(P,b))}_{\text{Transformed Point}} \tag{14}$$

Under this new perspective, provided by the transformation of the points through the expression (14), the measurements represented in Fig. 7 are transformed into the Figs. 8 where the response of the fiber

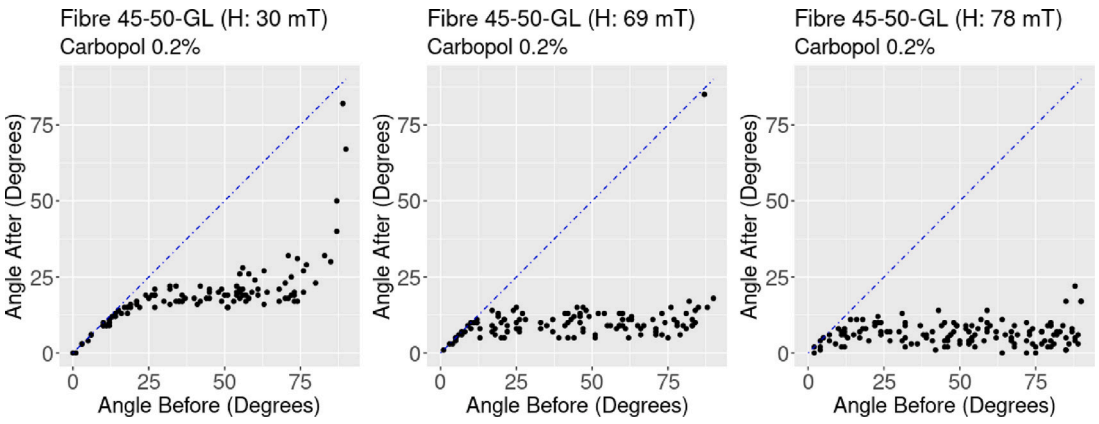

Fig. 7. Alignment process of measuring the angle θ before/after in Carbopol. Given example for 45-50 BL hooked-end steel fiber.

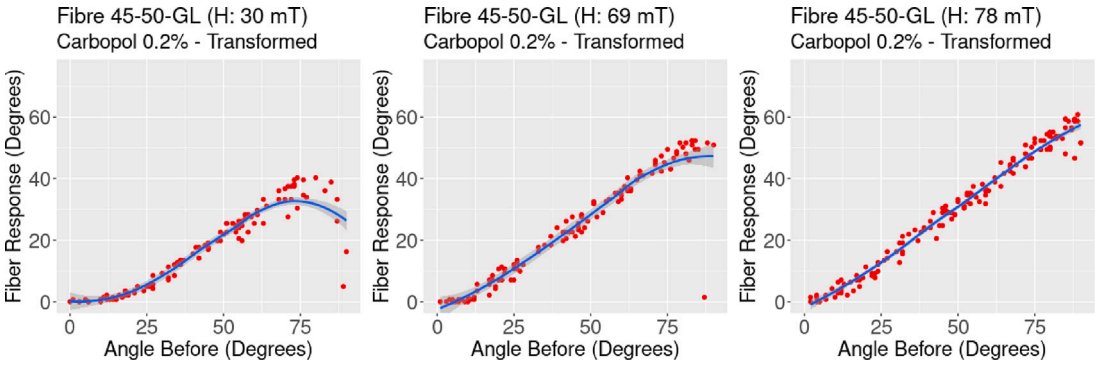

Fig. 8. Alignment process of measuring the angle θ before/after in Carbopol. Given example for 45-50 BL hooked-end steel fiber.

for each initial angle can be more rationally analyzed. Fig. 8 obtained after Eq. (14) transformation have been also smoothed using a locally estimated scatterplot smoothing (LOESS algorithm).

4.2. Statistical hypotheses & homogeneity in datasets

Using the specific methods of circular inferential statistics to the datasets obtained experimentally, some statements of interest can be determined with a certain degree of confidence. Moreover, there is already abundant literature about this issue of inferential statistics that can be applied as a useful tool for the purposes of the present work [27,28,31], which is based on circular data obtained.

The first statistical test focuses on determining whether the initial samples (before undergoing the magnetic pulse) correspond to distributions of homogeneous orientations along the circle (Hypothesis H_o), or on the contrary, there is a preferred direction (Reject the Hypothesis H_o). There are several tests of this type in circular statistics capable of determining homogeneity with a choosen confidence level p (p-value) of 5%. Some of these test include the Rayleigh test [28, 10.4] or the Kuiper test [28, 8.3.2], all of these homogeneity tests are suitable for cases in which the samples are distributed along all the circumference. But in our case, the measured angles are concentrated inside of 90 degree sector. To solve this situation an homogeneous sample of 100 values was generated using [32] and comparing with each sample due to *Watson's two-sample test of homogeneity* (aka *two sample* U^2 *statistic test*) [33]. This test has been run for each data pair between the homogeneous data generated and the fiber data before, a total of nine tests with the results shown in Table 3.

It is concluded, therefore, that the fiber orientation measurement experiments before being magnetically radiated are fairly homogeneous, that is, the null hypothesis H_o is then verified with a p-value of significance level equal to 0.05. Table 3 shows the U^2 value is less than the critical value in every row: then the null hypothesis cannot be dismissed. If U^2 greater than critical value: reject the null hypothesis, and conclude that the two samples differ significantly [31, ch 7.3] and [28, ch 8.3]. Since all the initial samples are homogeneous, it is possible, by symmetry, to reduce the orientations to the first quadrant.

Table 3
Test of homogeneity with significance level of the test: 0.05 comparing datasets after magnetic pulse: with initial remanency/no remanency.

Fiber	μ_oH	Test statistic	Critical value	H_o Hypothesis
45/50/BL	30 mT	0.1422	0.187	⇒ Do Not Reject
	69 mT	0.1278	0.187	⇒ Do Not Reject
	78 mT	0.0574	0.187	⇒ Do Not Reject
65/60/BG	30 mT	0.1798	0.187	⇒ Do Not Reject
	69 mT	0.1788	0.187	⇒ Do Not Reject
	78 mT	0.0359	0.187	⇒ Do Not Reject
80/60/BG	30 mT	0.1541	0.187	⇒ Do Not Reject
	69 mT	0.1485	0.187	⇒ Do Not Reject
	78 mT	0.1586	0.187	⇒ Do Not Reject

The second test carried out on the set of experimental data addresses the question: Are the data obtained from the initially magnetized fibers significantly different from the magnetized fibers? The *Watson's two-sample test of homogeneity* for circular data (aka *two sample* U^2 *statistic test*) [33] it has been applied to the paired samples of circular before/after datasets in the case of initially non-magnetized fiber versus initially remanent (magnetized) fiber. In the test, an p-value significance level equal to 0.001 has been chosen and the null hypothesis H_o of this test considers that both samples come from the same population or experiment.

If U^2 value is less than critical value: the null hypothesis cannot be dismissed. If U^2 greater than critical value: reject the null hypothesis, and conclude that the two samples differ significantly [31, ch 7.3]

Table 4
Watson's two-sample test of homogeneity with significance level of the test: 0.001 comparing datasets after magnetic pulse: with initial remanency/no remanency.

Fiber	μ_oH	Test statistic	Critical value	H_o Hypothesis
45/50/BL	30 mT	0.1239	0.385	⇒ Do Not Reject
	69 mT	0.1513	0.385	⇒ Do Not Reject
	78 mT	0.1134	0.385	⇒ Do Not Reject
65/60/BG	30 mT	0.2316	0.385	⇒ Do Not Reject
	69 mT	0.1749	0.385	⇒ Do Not Reject
	78 mT	0.1060	0.385	⇒ Do Not Reject
80/60/BG	30 mT	0.1112	0.385	⇒ Do Not Reject
	69 mT	0.0549	0.385	⇒ Do Not Reject
	78 mT	0.1070	0.385	⇒ Do Not Reject

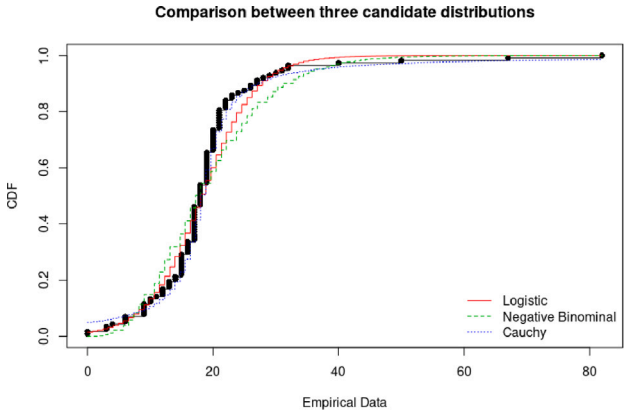

Fig. 9. Comparison of three CDF candidates to be the best fit.

and [28, ch 8.3]. The Watson test has been carried out for each pairing of experimental data of magnetized/non-Magnetized fiber (using R library from Agostinelli and Lund [32]) and the results are shown in the attached Table 4. The result of the test is that the null hypothesis cannot be rejected and therefore it can be stated that the initial magnetization of the fiber does not introduce a significant change in the response to different initial orientation angles.

The third statistical analysis of relevance carried out on the experimental data is to check whether or not the statistical datasets obtained after exposure to a magnetic pulse can fit to a specific distribution. Since it seems that the mean and median are very close in Table A.6, if not equal, the search for distributions that fit the experimental data is retrained only to symmetrical distributions. Another characteristic obtained in the experimental data that provides help to discriminate the search for a distribution is that there is always a small set of data around 90° (second dead zone), this situation means that there is always a kurtosis value. in the distribution that includes the value of 90° in its tail.

Among three selected candidates distributions due to likelihood: the Cauchy distribution, the negative binomial distribution and the logistic distribution were chosen. The maximum likelihood statistical method was chosen to estimate the needed parameters that fit the best to the empirical data. Once the parameters of the each three distributions was chosen by maximum likelihood estimation, they were compared against cumulative frequency graphs (CDF) for each type of fiber and magnetic field intensity. Finally, the distribution that fits the best to the three magnetic intensities was chosen. An example of CDF used in the comparison can be seen in Fig. 9.

The fit in the cumulative density distribution (CDF) of logistic distribution, after executing the maximum likelihood statistical method, shown in Fig. 9 the comparison between the three candidates. The logistic distribution has a better fit in those orientations close to the origin (first dead sector), as well as in the mean/median and therefore fits better in the quartiles. This logistic distribution also has a right tail

Table 5
The logistic distribution parameters for all the fiber types.

Fiber	RMS (mT)	μ (Median)	Scale
45/50/BL	30 mT	17.9°±0.6°	4.3 ± 0.3
	69 mT	9.4°±0.4°	2.3 ± 0.2
	79 mT	6.1°±0.3°	1.9 ± 0.1
65/60/BG	30 mT	27.5°±1.7°	10.4 ± 0.8
	69 mT	18.8°±0.8°	5.1 ± 0.4
	79 mT	16.6°±0.7°	5.1 ± 0.3
80/60/BG	30 mT	33.0°±2.0°	12.4 ± 0.9
	69 mT	22.2°±1.2°	7.0 ± 0.6
	79 mT	20.5°±0.9°	6.3 ± 0.4

that allows us to better describe those fibers orientations that are found in the area close to 90° (second dead sector). The logistic distribution has slightly longer tails compared to the normal distribution. The probability density function (PDF) of a logistic distribution is defined by Forbes et al. [34, ch. 28] as:

$$f(x \mid \mu, \sigma) = \frac{1}{4\sigma} \operatorname{sech}^2\left(\frac{x-\mu}{2\sigma}\right) \tag{15}$$

where μ is the location parameter and σ is the scale parameter. As μ decreases/increases, the PDF is shifted to the 0°/90°. As the scale σ decreases, the PDF gets pushed towards the mean, or it becomes narrower and taller; and contrary as σ increases, the PDF spreads out away from the mean, or it becomes broader and shallower. The median and the mode are always equal to the mean in the logistic distribution [34, ch. 28] and the standard distribution of logistic is equal to $\sigma\pi\sqrt{3}/3$. Therefore the logistic distribution has been chosen for every case studied (magnetic field and fiber type). The results obtained for the two parameters: μ and σ are presented according to the maximum likelihood statistical method for this distribution in Table 5.

In Table 5 it can be seen that μ is identified with the angle of the median (or equivalently with the median). The equivalence between the mean and the median can be verified on represented values of mean and median (50% quartile) for each type of fiber in Table A.6 . On the other hand, the scale in the logistic distribution, indicated by the letter σ, controls the width of the distribution. It can be seen that the scale is reduced when the magnetic intensity increases; this reduction in the sigma scale is verified for all types of fibers. This downscaling phenomenon indicates that the orientations of the fibers tend to concentrate preferably at the mean angle $\bar{\theta}$, as shown graphically in Fig. 6 that belongs to the circular histogram before/after the fiber 45/50/BL has been exposed to pulse.

According to these two parameters (see Table 5), the fiber with the best response will be the one that leaves the median μ closer to zero (coil axis) and that also has a smallest scale σ, that is, with a greater concentration of fibers oriented around the mean. The best response, according to this analysis, is the 45/50/BG steel fiber at high/medium magnetic field intensities; the 80/60/BG fiber produces less alignment and is more dispersed than the rest of the fiber types.

5. Analysis of experimental results

With respect to the descriptive circular statistics the tables shown in Appendix, the following phenomena can be verified that deserve comments.

1. It has been shown (hypothesis H_o of homogeneity for the all initial samples, described in Table 3) that the initial samples are homogeneous, that is, they distribute their initial orientation fairly with a 5% of confidence level (p-value). On the other hand, because the angles of fiber orientation has been reduced, by symmetry, to a single quadrant of the circumference, the mean circular direction $\bar{\theta}$ of each sample before being magnetically radiated is always close to approximately 45° (homogeneous mean

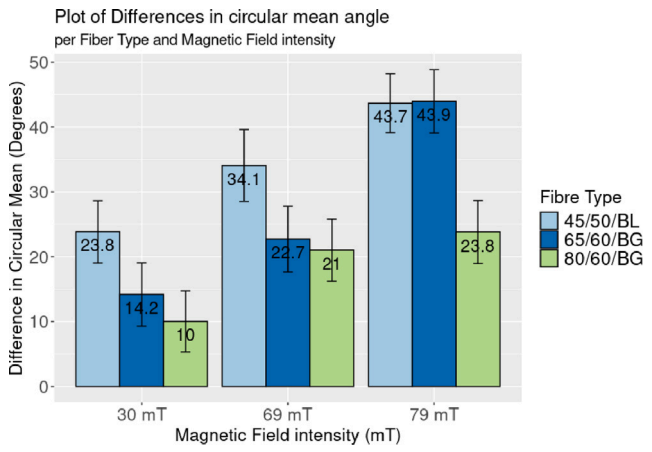

Fig. 10. Change in mean/median $\Delta\bar{\theta}$ in Table A.6 with circular standard deviation error.

value). This values of mean angle $\bar{\theta}$ can be seen in Tables A.6 and A.7 in the row labeled 'before' for each fiber and magnetic field strength. Table A.7 of magnetized fiber data has a greater dispersion around 45° compared to non-magnetized data because a smaller amount of data (data size) are involved in the circular statistics.

Once the fibers have been subjected to a magnetic pulse, the steel fibers concentrate their orientation around a characteristic mean direction $\bar{\theta}$ (see Fig. 6). This phenomenon of change in mean orientation seems to have dependency on: type of fiber, intensity of the magnetic field, and it is assumed that also with the rheological characteristics of the fluid matrix. This mean direction tends to be aligned with the magnetic axis of the coil ($\theta \rightarrow 0°$), and can be seen in Tables A.6 and A.7 that all the fibers tend to zero after be magnetically radiated, with tendency greater when greater the intensity of the peak of the magnetic field.

When the differences between the circular means before/after being magnetically radiated (shown in Table A.6 under the column $\bar{\theta}$) are analyzed, the difference value $\Delta\bar{\theta}$ obtained can be shown in Fig. 10 for each magnetic field intensity and fiber type. The figure includes the circular standard deviation which is approximately 4° for each mean orientation. By subtracting the average before being radiated, considered an initial homogeneous distribution close to 45°, and the final average value after being radiated, this difference is proportional to the average response of the fiber. It can be seen in Fig. 10 comparing the difference between the circular mean orientation after the magnetic pulse that the fiber response grows with the intensity of the magnetic peak. In the three cases of magnetic field intensity, 45/50/BL is the type of fiber that responds best, followed by 65/60/GL and finally by 80/60/GL, which shows lower responses to the magnetic pulse.

2. The circular mean and the median are close together in all the cases. Then we can affirm that all the data set has a symmetrical distribution. The calculated circular standard deviation is approximately 4° and represented in Fig. 10 allowing us to verify in the Tables A.6 and A.7 that the circular average orientation angle $\bar{\theta}$ and the median angle can be coincident.
3. Figs. 6 are circular histograms that show the stacked orientations of the steel fibers on their perimeter, bins of 5 degrees of amplitude have been considered. Each bin indicates the relative fraction of fiber orientation χ_k that possesses the characteristic orientation θ_k of the middle of the bin window. That is, 2.5°, 7.5°, 12.5°, etc. Fig. 6 shows that the relative orientation fraction is concentrated, after the magnetic pulse, around the average orientation angle as well as the median.
4. In Fig. 8 it can be observed that there is always a fraction of the steel fiber, whose limiting angle θ_1 is close to the magnetic axis of the coil, which does not undergo alignment (first dead sector). These fibers correspond to points in Fig. 8 that are located close to the bisector line at angles close to 0°. The proximity to the bisector indicates that they do not show alignment response. There is, for each type of steel fiber, an angular value of theta1 orientation from which the fibers begin to show an alignment response to the magnetic field. This angle will be called the effective start of the window. This effective window starts in a angle (θ_1) taht can clearly be considered as a specific transition orientation: fibers with an alignment angle below θ_1 will not undergo an alignment process, however those that exceed this angle will respond to the magnetic field (Fig. 11). It can be seen that the θ_1 angle will be smaller the greater the intensity of the magnetic field, increasing the width of the effective window to the population of fibers. Simulations performed according with section §2.3 shows that this limiting angle θ_1 is proportional to the static yield stress of the fluid matrix. It is logical to think that the greater this static yield stress, and the magnetic torque being proportional to the alignment angle, only those fibers with greater alignment angles will undergo through the alignment process by overcoming the static stress of the fluid.
5. Fibers with orientation angles perpendicular to the coil axis do not appear to be affected by magnetic torque. For this reason, a tendency is shown in Figs. 8 towards the bisector at angles close to 90°. The Eq. (1) shows that the magnetic torque exerted on the steel fiber shows a maximum at values close to 90° to immediately decrease, this decrease in Torque causes these fibers to be unable to rotate due to the presence of a static yield stress that prevents the fiber from rotating. This process indicates that there is also a transition angle θ_2 close to 90° (perpendicular to the axis of the coil) such that fibers with orientations below this value have alignment response, while fibers that are $\theta_2 < \theta < 90°$ do not rotate (second dead sector). The simulations show that the amplitude of this second window will depend on the cohercive field of the ferromagnetic material of the fiber, as a general rule is approximately 200 A/m, the amplitude of this window in most fibers will be close to two degrees (depending on the static yield stress). Thus, it is concluded that the effective response window for orientation alignment of steel fibers is a orientation amplitude that satisfies:

$$\text{Effective Window:} \qquad \theta_1 \leq \theta < \theta_2 \tag{16}$$

Where θ is the initial fiber orientation, and θ_1, θ_2 are the transition angles where aligning, or not, the steel fiber. The window of effectiveness thus defined becomes wider as the magnetic intensity peak becomes more intense. This phenomenon of the existence of an effective window can be seen in the datasets represented in Figs. 8 where the angular response of the steel fiber is shown.
6. The response of the fiber, shown in Figs. 8, show in all fiber types the same pattern, the higher the magnetic field intensity the straighter it is. Showing a greater response of the fiber at values close to 90°. In cases of low field intensity, a curvature can be observed due mainly to the presence of ferromagnetic hysteresis characteristics.

In relation to the circular histogram in Fig. 6, it can be seen that the fibers are concentrated around certain angular values. The before/after fiber distribution can be better and summarized described using the quartiles 25, 50, 75, 100 m as shown in the Tables A.6, A.7. The distribution that best fits these data is the logistic one according to the Table 5.

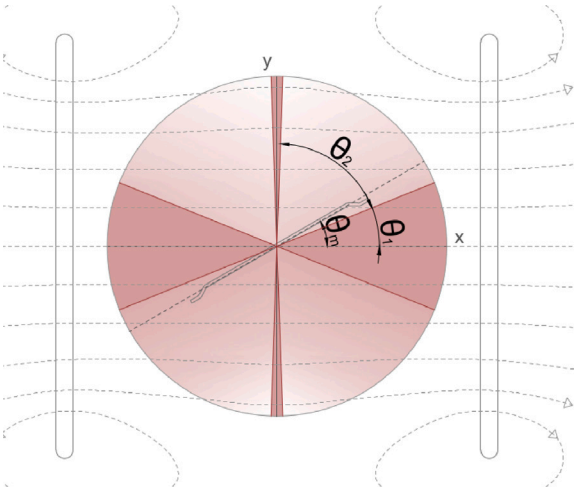

Fig. 11. The dead/active sectors within the circle showing the reference angles θ_1 and θ_2 as well as the average/median angle $\bar{\theta}$ of fiber distribution.

Concerning the results obtained to discriminate the effects in fiber rotation between initially state magnetized/non-magnetized we conclude that a magnetic peak profile from a RCL discharge (Fig. 3) with a maximum intensity at 0.01 s it is, in any case, a sufficient time interval to reach the saturated magnetic field B_m (Fig. 1), independent of the initial state of the fiber (whether magnetized or with remanence). This statement is true in each of the experiments described, because the magnetic intensity of the coil (see Table 1) is always several tens of mT, a magnetic induction more than enough to set up the fiber to its magnetic saturation at 0.01 s. When the peak of magnetic intensity occurs, the driving torque is maximum and the fiber is already magnetically saturated, and it is precisely at this moment when the fiber aligns with the axis of the coil (it became an active fiber), always that the fiber has exceeded the static yield stress τ_0. In the case that the magnetic torque does not exceed the static yield stress, the fiber is said to be a dead fiber, not responding with rotation to the pulse.

The efficiency factor proposed by Krenchel η_θ (as shown in the expression (13)) used here as a measure of the general orientation of the steel fibers, due in part to the fact that it brings together and encodes all those relevant parameters of the statistical analysis: the angular fraction χ_k per representative k-bins obtained from the circular percentiles of the fiber orientation distribution. This efficiency factor η_θ has been calculated using (13) taking the magnetic axis of the coil as a reference and its value can be found in the last column of Tables A.6 and A.7 for all cases of fiber type and magnetic field intensities. The η_θ efficiency values obtained in Tables A.6 and A.7 are in line with the values discussed on the parameters of Table 5 relative to the logistic distribution. It can be verified again that 45/50/BL steel fiber at a medium/high magnetic intensity offers the best efficiency among all types of fibers. As can be observed in Fig. 4, this fiber is the second with higher magnetic torque, it is very possible that its own slenderness favors it with a lower opposing rheological torque, something that can be affirmed by verifying that it is precisely this fiber that is the most concentrated around the mean/circular median, as seen in Table 5. Returning to the discussion about the efficiency factor, this factor value does not explicitly provide the density of orientations around the mean (as the scale σ of the logistic distribution does), but it has the advantage of being introduced into the 'rule of mixtures' and thus predicting the value of Young's modulus or elastic behavior of a material with fibers (Eq. (12)).

6. Summary and conclusions

After analyzing the results, it can be verified that a magnetic pulse aligns the homogeneous fraction of fibers in a preferred direction that coincides with the mean (or equivalently also the median) directional direction. Likewise, due to the rheological properties of the fluid matrix, such as static yield stress (τ_o), two 'dead angle intervals' (dead sectors) arise in which the steel fibers do not rotate. The first dead sector of interest corresponds to angles close to the axis of the coil, and the second narrowest sector is found at angles close to perpendicular to the axis of the coil. These two dead sectors are based on the magnetic torque exerted on the steel fiber that does not exceed the value of the static yield stress and therefore there will be a fraction of fiber during a magnetic pulse that will not respond with alignment. The presence of these two dead sectors has great relevance in the alignment processes; their amplitude will be a function of the intensity of the coil, the ferromagnetic properties of the steel fiber and the rheological properties of the fluid.

The first dead sector is always wider than the second, and is caused because the fiber orientation angles close to zero (aligned with the coil) do not cause a magnetic torque capable of causing the fiber to rotate and align, this 'insufficient' magnetic torque does not exceed the opposing rheological torque of the fluid that surrounds it. The second dead sector perpendicular to the coil axis is caused by the intrinsic ferromagnetic properties of the fiber, and will always be narrower than the first sector (generally two to five degrees wide). As a general rule, the higher the magnetic intensity of the coil, the narrower both dead sectors become. And in another way, the greater the static yield stress of the fluid, the larger the two dead sectors will be. It is understood that vibration operations reduce static tension, and therefore these dead sectors see their amplitude reduced if magnetic exposure were carried out during this compaction process. The hysteresis loop, being understood as the coding ferromagnetic properties of the steel fiber, affects the amplitude of the dead sectors very subtly, for example the second dead sector (perpendicular to the coil) is wider when cohercive field of the hysteresis loop is larger.

All experiments carried out initially started from a homogeneous distribution of fiber orientations. After the fibers are exposed to the magnetic pulse, it has been proven that the resulting distribution of orientations corresponds to a logistic distribution. This characteristic distribution is used to describe systems of opposite natures, such as describing global population growth in the face of limited resources. The logistic distribution emerges here due to the confrontation between driving magnetic torques and resisting rheological torques. In future research, the objective is to determine the relationship of the parameters of this distribution with the rheological properties of the fluid matrix and the magnetic properties of the steel fiber.

Dead sector circles can be a very useful tool because they are suitable for managing alignment sequences. Because a single exposure results in two dead sectors and a predominant misaligned mean (median) direction with respect to the coil axis, it is conceivable that there can be a series (or sequences) of successive rotations of the coil axis, or sample rotations, capable of optimizing the alignment process, moving fibers from dead sectors to active sectors in each rotation, thus achieving an optimal final effect. Directional statistics, used here for the first time, have a fundamental role in alignment management in composites because they can help precisely plan alignment/rotation sequences. This is due to the property of all elements of directional statistics being rotationally equivariant: means, medians, quartiles, etc.

The results obtained in this work have focused mainly on the use of a fluid metaphor (carbopol) that presents a static yield stress similar to that of mortars. The study carried out on real cementitious materials can provide a result similar to the one obtained in relation to the angular magnitude of the two dead sectors (which have a relationship with τ_o), but it is possible that since the mortars are fluid that follow a Bingham-type rheological law, the composition of the quartiles is certainly different, and in the same way the logistic distribution may not be the predominant one. However, this issue is the subject of future work, in which other rheological parameters can be considered.

Table A.6
Table of descriptive circular statistics for fibers initially without magnetization.

Fiber	Sequence	μ_oH (RMS)	N	$\sin\bar{\theta}$	$\cos\bar{\theta}$	$\bar{\theta}$	$\bar{R}$	25%	50%	75%	100%	η_θ
45/50/BL	Before	30 mT	112	0.6165	0.6729	42.5°	0.914	19.0°	45.0°	60.0°	90.0°	0.387
45/50/BL	After	30 mT	112	0.3149	0.9327	18.6°	0.984	15.0°	18.0°	21.0°	82.0°	0.782
45/50/BL	Before	69 mT	113	0.6258	0.6487	43.9°	0.901	21.0°	44.5°	65.7°	90.0°	0.383
45/50/BL	After	69 mT	113	0.1706	0.9771	9.9°	0.992	7.0°	9.0°	11.7°	85.0°	0.926
45/50/BL	Before	78 mT	140	0.6888	0.5779	50.0°	0.899	27.0°	52.0°	74.0°	90°	0.313
45/50/BL	After	78 mT	140	0.1102	0.9918	6.3°	0.998	4.0°	6.0°	9.0°	22.0°	0.964
Fiber	Sequence	μ_oH (RMS)	N	$\sin\bar{\theta}$	$\cos\bar{\theta}$	$\bar{\theta}$	$\bar{R}$	25%	50%	75%	100%	η_θ
65/60/BG	Before	30 mT	106	0.6115	0.6406	43.6°	0.885	18.2°	42.5°	66.7°	90.0°	0.408
65/60/BG	After	30 mT	106	0.4646	0.8214	29.5°	0.944	16.0°	28.0°	35.7°	89.0°	0.583
65/60/BG	Before	69 mT	113	0.6092	0.6789	41.9°	0.912	22.0°	41.0°	60.0°	89.0°	0.398
65/60/BG	After	69 mT	113	0.3236	0.9293	19.2°	0.984	14.0°	19.0°	25.0°	87.0°	0.767
65/60/BG	Before	78 mT	147	0.6964	0.5784	50.3°	0.905	31.5°	52.0°	72.0°	90°	0.296
65/60/BG	After	78 mT	147	0.2968	0.9347	17.6°	0.981	12.0°	16.0°	22.0°	88.0°	0.797
Fiber	Sequence	μ_oH (RMS)	N	$\sin\bar{\theta}$	$\cos\bar{\theta}$	$\bar{\theta}$	$\bar{R}$	25%	50%	75%	100%	η_θ
80/60/BG	Before	30 mT	118	0.6165	0.6382	44.1°	0.887	19.0°	43.5°	69.0°	89.0°	0.396
80/60/BG	After	30 mT	118	0.5215	0.7733	33.9°	0.933	18.0°	32.1°	47.7°	87.7°	0.501
80/60/BG	Before	69 mT	99	0.6175	0.6438	43.8°	0.829	16.0°	42.5°	70.5°	90.0°	0.388
80/60/BG	After	69 mT	99	0.3763	0.8749	22.8°	0.971	13.0°	23.0°	28.7°	88.0°	0.695
80/60/BG	Before	78 mT	147	0.6166	0.6298	44.4°	0.881	15.5°	44.0°	70.0°	90°	0.390
80/60/BG	After	78 mT	147	0.3445	0.9182	20.6°	0.981	12.5°	21.0°	27.0°	69.0°	0.731

Table A.7
Table of descriptive circular statistics for fibers initially with magnetic remanency (magnetized).

Fiber	Sequence	μ_oH (RMS)	N	$\sin\bar{\theta}$	$\cos\bar{\theta}$	$\bar{\theta}$	$\bar{R}$	25%	50%	75%	100%	η_θ
45/50/BL	Before	30 mT	22	0.6344	0.6649	43.6°	0.914	23.0°	40.0°	61.2°	87.0°	0.391
45/50/BL	After	30 mT	22	0.3928	0.8876	23.8°	0.971	18.2°	20.5°	26.7°	87.0°	0.699
45/50/BL	Before	69 mT	21	0.8045	0.4434	61.1°	0.918	44.0°	68.0°	79.0°	90.0°	0.87
45/50/BL	After	69 mT	21	0.2141	0.9755	12.4°	0.998	10.0°	12.0°	14.0°	17.0°	0.897
45/50/BL	Before	78 mT	33	0.5384	0.7457	35.8°	0.919	18.0°	31.0°	46.0°	88°	0.115
45/50/BL	After	78 mT	33	0.1279	0.9902	7.4°	0.998	6.0°	8.0°	9.0°	13.0°	0.225
Fiber	Sequence	μ_oH (RMS)	N	$\sin\bar{\theta}$	$\cos\bar{\theta}$	$\bar{\theta}$	$\bar{R}$	25%	50%	75%	100%	η_θ
65/60/BG	Before	30 mT	19	0.6543	0.6440	45.4°	0.918	30.5°	36.0°	70.0°	84.0°	0.358
65/60/BG	After	30 mT	19	0.5901	0.8381	31.3°	0.981	25.5°	29.0°	39.0°	51.0°	0.535
65/60/BG	Before	69 mT	25	0.6431	0.6566	44.4°	0.919	29.0°	38.0°	59.0°	89.0°	0.374
65/60/BG	After	69 mT	25	0.4087	0.8893	24.7°	0.978	19.0°	24.0°	28.0°	72.0°	0.665
65/60/BG	Before	78 mT	29	0.5628	0.7548	36.7°	0.941	21.0°	34.0°	47.0°	83.0°	0.451
65/60/BG	After	78 mT	29	0.2508	0.9639	14.6°	0.996	12.0°	15.0°	16.0°	26.0°	0.849
Fiber	Sequence	μ_oH (RMS)	N	$\sin\bar{\theta}$	$\cos\bar{\theta}$	$\bar{\theta}$	$\bar{R}$	25%	50%	75%	100%	η_θ
80/60/BG	Before	30 mT	24	0.6189	0.6982	41.5°	0.933	25.7°	36.0°	54.0°	89.0°	0.390
80/60/BG	After	30 mT	24	0.5647	0.7729	36.1°	0.957	24.0°	32.1°	44.1°	85.2°	0.458
80/60/BG	Before	69 mT	18	0.5879	0.6676	41.4°	0.889	25.0°	32.0°	64.0°	90.0°	0.452
80/60/BG	After	69 mT	18	0.4009	0.8969	24.1°	0.982	22.3°	24.5°	31.7°	42.0°	0.660
80/60/BG	Before	78 mT	31	0.6011	0.6539	42.6°	0.888	18.0°	41.0°	65.0°	86.0°	0.412
80/60/BG	After	78 mT	31	0.3371	0.9253	20.1°	0.984	14.0°	21.0°	25.0°	49.0°	0.743

CRediT authorship contribution statement

Víctor Pérez Villar: Writing – original draft, Validation, Methodology, Investigation, Formal analysis, Data curation, Conceptualization. **Nelson Flores Medina:** Writing – review & editing, Supervision, Methodology, Investigation, Funding acquisition, Conceptualization. **Laura Trigo Ramirez:** Writing – review & editing, Methodology, Investigation, Data curation.

Declaration of competing interest

The authors declare the following financial interests/personal relationships which may be considered as potential competing interests: Nelson flores medina reports financial support and administrative support were provided by Ministry of Science Technology and Innovations. If there are other authors, they declare that they have no known competing financial interests or personal relationships that could have appeared to influence the work reported in this paper.

Data availability

Data will be made available on request.

Acknowledgments

This research was funded by the Spanish Science Ministery, grant number PID2020-119707RB-I00 (ORIENTACIÓN DE FIBRAS DE REFUERZO EN HORMIGÓN PARA EDIFICACIÓN MEDIANTE CAMPOS MAGNÉTICOS). Support from the Universidad de las Palmas de Canaria in also highly acknowledged.

Appendix. Descriptive circular statistics based on experimental data

See Tables A.6 and A.7.

References

[1] M.J. Peterman, Method of aligning magnetic particles in a non-magnetic matrix, 1945, US2849312A.

[2] G.M. Knoblach, Using electric fields to control fiber orientation during the manufacturing of composite materials, SAMPE J. 25 (6) (1989) 9–16.

[3] A. Miller, F. Björklund, Method of reinforcing concrete with fibres, 1977, Patent: US 4062913 A.

[4] M. Wijffels, R. Wolfs, A. Suiker, T. Salet, Magnetic orientation of steel fibres in self-compacting concrete beams: Effect on failure behaviour, Cem. Concr. Compos. 80 (2017) 342–355, http://dx.doi.org/10.1016/j.cemconcomp.2017.04.005.

[5] M.M. Al Rifai, K.S. Sikora, M.N. Hadi, Magnetic alignment of micro steel fibers embedded in self-compacting concrete, Constr. Build. Mater. 412 (2024) 134796, http://dx.doi.org/10.1016/j.conbuildmat.2023.134796.

[6] R. Mu, R. Dong, H. Liu, H. Chen, Q. Cheng, C. Fan, Preparation of aligned steel-fiber-reinforced concrete using a magnetic field created by the assembly of magnetic pieces, Crystals 11 (7) (2021) http://dx.doi.org/10.3390/cryst11070837.

[7] B. Boulekbache, M. Hamrat, M. Chemrouk, S. Amziane, Flowability of fibre-reinforced concrete and its effect on the mechanical properties of the material, Constr. Build. Mater. 24 (9) (2010) 1664–1671, http://dx.doi.org/10.1016/j.conbuildmat.2010.02.025.

[8] J. Spangenberg, N. Roussel, J. Hattel, H. Stang, J. Skocek, M. Geiker, Flow induced particle migration in fresh concrete: Theoretical frame, numerical simulations and experimental results on model fluids, Cem. Concr. Res. 42 (4) (2012) 633–641, http://dx.doi.org/10.1016/j.cemconres.2012.01.007.

[9] G.K. Auernhammer, S. Fataei, M.A. Haustein, H.P. Patel, R. Schwarze, E. Secrieru, V. Mechtcherine, Transparent model concrete with tunable rheology for investigating flow and particle-migration during transport in pipes, Mater. Des. 193 (2020) 108673, http://dx.doi.org/10.1016/j.matdes.2020.108673.

[10] Z. Jaworski, T. Spychaj, A. Story, G. Story, Carbomer microgels as model yield-stress fluids, Rev. Chem. Eng. 38 (7) (2022) 881–919, http://dx.doi.org/10.1515/revce-2020-0016.

[11] R. Gettu, D. Gardner, H. Saldívar, B. Barragán, Study of the distribution and orientation of fibers in SFRC specimens, Mater. Struct./Materiaux Constr. 38 (275) (2005) 31–37, http://dx.doi.org/10.1617/14021, Cited by: 162.

[12] F. Laranjeira, S. Grünewald, J. Walraven, et al., Characterization of the orientation profile of steel fiber reinforced concrete, Mater. Struct. (44) (2011) 1093–1111, http://dx.doi.org/10.1617/s11527-010-9686-5.

[13] F. Laranjeira, A. Aguado, C. Molins, S. Grünewald, J. Walraven, S. Cavalaro, Framework to predict the orientation of fibers in FRC: A novel philosophy, Cem. Concr. Res. 42 (6) (2012) 752–768, http://dx.doi.org/10.1016/j.cemconres.2012.02.013.

[14] A. Abrishambaf, M. Pimentel, S. Nunes, Influence of fibre orientation on the tensile behaviour of ultra-high performance fibre reinforced cementitious composites, Cem. Concr. Res. 97 (2017) 28–40, http://dx.doi.org/10.1016/j.cemconres.2017.03.007.

[15] S. Lorente, S. Carmona, C. Molins, Use of fiber orientation factor to determine residual strength of steel fiber reinforced concrete, Constr. Build. Mater. 360 (2022) 128878, http://dx.doi.org/10.1016/j.conbuildmat.2022.128878.

[16] H.L. Cox, The elasticity and strength of paper and other fibrous materials, Br. J. Appl. Phys. 3 (3) (1952) 72, http://dx.doi.org/10.1088/0508-3443/3/3/302.

[17] H. Krenchel, Fibre reinforcement; theoretical and practical investigations of the elasticity and strength of fibre-reinforced materials, 1964.

[18] I.P. eć, P. Hine, M. Bonner, I. Ward, D. Barton, Die drawn wood polymer composites. II. Micromechanical modelling of tensile modulus, Compos. Sci. Technol. 70 (1) (2010) 53–60, http://dx.doi.org/10.1016/j.compscitech.2009.09.004.

[19] R. Mu, J. Chen, X. Chen, C. Diao, X. Wang, L. Qing, Effect of the orientation of steel fiber on the strength of ultra-high-performance concrete (UHPC), Constr. Build. Mater. 406 (2023) 133431, http://dx.doi.org/10.1016/j.conbuildmat.2023.133431.

[20] A. Raju, M. Shanmugaraja, Recent researches in fiber reinforced composite materials: A review, Mater. Today: Proc. 46 (2021) 9291–9296, http://dx.doi.org/10.1016/j.matpr.2020.02.141, International Mechanical Engineering Congress 2019.

[21] J.R. Reitz, F.J. Milford, R.W. Christy, Foundations of electromagnetic theory, first ed., in: Series in Physics, Addison-Wesley Publishing Company, Massachusetts, EEUU, 1960.

[22] K. Künzel, V. Papež, K. Carrera, R. Sovják, Magnetic properties of steel fibres commonly used in concrete, Mater. Today: Proc. 62 (2022) 2599–2603, http://dx.doi.org/10.1016/j.matpr.2022.04.134, 37th Danubia Adria Symposium on Advances in Experimental Mechanics.

[23] R. Jastrzębski, K. Chwastek, Analytical expressions for magnetization curve, in: 2017 Progress in Applied Electrical Engineering, PAEE, 2017, pp. 1–4, http://dx.doi.org/10.1109/PAEE.2017.8009019.

[24] J. Rivas, J. Zamarro, E. Martin, C. Pereira, Simple approximation for magnetization curves and hysteresis loops, IEEE Trans. Magn. 17 (4) (1981) 1498–1502, http://dx.doi.org/10.1109/TMAG.1981.1061241.

[25] J. Takács, Mathematics of hysteretic phenomena : the T(x) model for the description of hysteresis, 2003, http://dx.doi.org/10.1002/3527606521.

[26] P. Banfill, G. Tattersall, Rheology of fresh cement and concrete, Rheol. Rev. 44 (6) (2006) 61–130, http://dx.doi.org/10.1617/s11527-010-9686-5.

[27] N.I. Fisher, Statistical Analysis of Circular Data, Cambridge University Press, 1993, http://dx.doi.org/10.1017/CBO9780511564345.

[28] K.V. Mardia, P.E. Jupp, Directional statistics, First, in: Willey Series in Probability and Statistics, John Wiley & Sons, Ltd., London, 2000, http://dx.doi.org/10.1002/9780470316979.

[29] H. Krenchel, Fibre spacing and specific fibre surface, Fibre Reinf. Cem. Concr. 1975 (1975) 69–79.

[30] L. Martinie, P. Rossi, N. Roussel, Rheology of fiber reinforced cementitious materials: classification and prediction, Cem. Concr. Res. 40 (2) (2010) 226–234, http://dx.doi.org/10.1016/j.cemconres.2009.08.032.

[31] S.R. Jammalamadaka, A. SenGupta, Topics in Circular Statistics, First, World Scientific, 2001, http://dx.doi.org/10.1142/4031.

[32] C. Agostinelli, U. Lund, R package `circular`: Circular statistics (version 0.5-0), 2023, URL https://CRAN.R-project.org/package=circular.

[33] J. Zar, Watson's nonparametric two-sample test, Behav. Res. Methods Instrum. 8 (1976) http://dx.doi.org/10.3758/BF03202199, 513–513.

[34] C. Forbes, M. Evans, N. Hastings, B. Peacock, Statistical Distributions, John Wiley & Sons, Ltd, 2010, pp. 127–130, http://dx.doi.org/10.1002/9780470627242.ch28.